

# CORE: Robust Out-of-Distribution Detection via Confidence and Orthogonal Residual Scoring

Jin Mo Yang<sup>1</sup>, Hyung-Sin Kim<sup>1</sup>, and Saewoong Bahk<sup>1</sup>

Seoul National University, Seoul, South Korea  
{jmyang, hyungkim, sbahk}@snu.ac.kr

**Abstract.** Out-of-distribution (OOD) detection is essential for deploying deep learning models reliably, yet no single method performs consistently across architectures and datasets—a scorer that leads on one benchmark often falters on another. We attribute this inconsistency to a shared structural limitation: logit-based methods see only the classifier’s confidence signal, while feature-based methods attempt to measure membership in the training distribution but do so in the full feature space where confidence and membership are entangled, inheriting architecture-sensitive failure modes. We observe that penultimate features naturally decompose into two orthogonal subspaces: a classifier-aligned component encoding confidence, and a residual the classifier discards. We discover that this residual carries a class-specific directional signature for in-distribution data—a membership signal invisible to logit-based methods and entangled with noise in feature-based methods. We propose *CORE* (COnfidence + REsidual), which disentangles the two signals by scoring each subspace independently and combines them via normalized summation. Because the two signals are orthogonal by construction, their failure modes are approximately independent, producing robust detection where either view alone is unreliable. *CORE* achieves competitive or state-of-the-art performance across five architectures and five benchmark configurations, ranking first in three of five settings and achieving the highest grand average AUROC with negligible computational overhead.

**Keywords:** Out-of-distribution detection · Model reliability · Anomaly detection · Feature space analysis

## 1 Introduction

Out-of-distribution (OOD) detection is essential for deploying deep learning models reliably in open-world environments [30]. Among the many proposed approaches, *post-hoc* scoring methods are particularly attractive: they require no retraining, apply to any pretrained classifier, and operate at negligible cost during inference [10, 16]. Yet a persistent and under-discussed problem remains—**no single post-hoc method is reliably the best across architectures and datasets**. Energy [16] dominates on some benchmarks, KNN [23] on others, ViM [26] on yet others. A method that ranks first in one setting can drop to

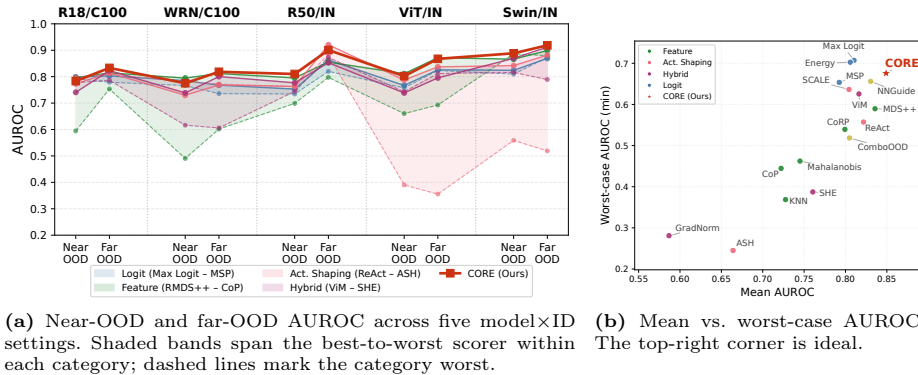


**Fig. 1: Fragility of post-hoc OOD scorers across architectures and datasets.** Catastrophic failures occur systematically for activation-shaping and feature-based methods on specific architectures (e.g., ViT/IN, Swin/IN). *CORE* (red) is consistently the most robust scorer across all settings.

mediocre performance in the next. For practitioners, this inconsistency is a serious obstacle: without knowing which OOD inputs will be encountered, there is no principled way to choose a scorer.

Figure 1 shows the comprehensive picture. We evaluate the best and worst scorers from each of five baseline categories—logit-based, feature-based, activation shaping, hybrid, and score combination—across five model×ID configurations with both near-OOD and far-OOD benchmarks (Fig. 1a). Shaded bands show the full range within each category. Catastrophic failures are systematic, not isolated: activation-shaping methods collapse on ViT/ImageNet and Swin/ImageNet, while feature-based methods exhibit wide variance across all settings. Fig. 1b summarizes each scorer by its mean and worst-case AUROC: *CORE* (red star) sits in the upper-right corner, achieving the highest mean AUROC while maintaining the best worst case. The question is: *why does every category have a blind spot, and can we close them?*

Existing methods each rely on a different criterion—and each breaks down in certain settings (Fig. 2). Logit-based methods [10, 16] measure *confidence* but are blind to OOD samples that produce confident predictions (Fig. 2a). Feature-based methods [14, 23] measure *membership* via distances in feature space, but operate on the full  $z$  where confidence and membership are entangled, inheriting architecture-sensitive pathologies such as hubness (Fig. 2b). Activation shaping methods [6, 22] denoise features before recomputing logits, but their heuristics vary across architectures (Fig. 2c).

The common thread is that the feature  $z$  carries two distinct signals—confidence and membership—and no existing method cleanly separates them. We formalize this observation. A classifier’s final linear layer computes logits  $\ell = Wz$ , where  $W \in \mathbb{R}^{C \times d}$  and  $z \in \mathbb{R}^d$  is the penultimate feature. This operation is a projection: it uses only the component of  $z$  aligned with class weight

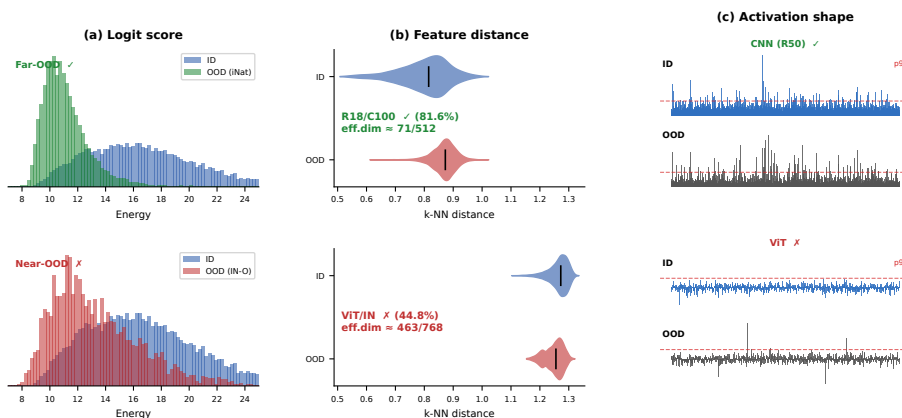


**Fig. 2:** Each column represents one scorer category: (a) logit-based energy score (far-OOO separates, near-OOO overlaps), (b) feature-based k-NN distance (R18/C100 separates, ViT/IN concentrates), (c) per-unit penultimate activations (CNN shows sparse OOD spikes above the ReAct threshold; ViT activations are symmetric with no clear ID/OOD separation). Top rows: settings where the approach succeeds; bottom rows: where it fails.

directions. We can decompose any feature  $z$  with respect to its predicted class  $\hat{y}$  into two orthogonal components:

$$z = z_{\parallel} + z_{\perp}, \quad z_{\parallel} = \frac{z \cdot w_{\hat{y}}}{\|w_{\hat{y}}\|^2} w_{\hat{y}}, \quad z_{\perp} = z - z_{\parallel}, \quad (1)$$

where  $w_{\hat{y}}$  is the classifier weight for the predicted class. The parallel component  $z_{\parallel}$  determines the logit magnitude—it encodes *confidence*. The orthogonal residual  $z_{\perp}$  is everything the classifier discards.

Through this lens, the blind spots identified above become precise: logit-based methods see only  $z_{\parallel}$ ; feature-based methods measure membership in the full  $z$  where it is entangled with  $z_{\parallel}$ ; activation shaping modifies  $z$  to improve  $z_{\parallel}$  but never accesses  $z_{\perp}$ . No existing method scores  $z_{\perp}$  independently.

**Key finding: structured residual.** We discover that  $z_{\perp}$  carries a *class-specific directional signature* for in-distribution data. Within each predicted class  $c$ , ID samples’ residuals  $z_{\perp}$  consistently align with a characteristic mean direction  $\mu_{\perp}^{(c)}$ , estimated from as few as  $\sim 13$  training samples per class. OOD samples’ residuals do not exhibit this alignment. A single cosine similarity  $\cos(z_{\perp}, \mu_{\perp}^{(\hat{y})})$  is therefore a powerful *membership* signal—one that is entirely invisible to logit-based methods and entangled with noise in feature-based methods.

**Why combining works: orthogonal decoupling.** Because  $z_{\parallel} \perp z_{\perp}$  by construction, the confidence signal (Energy score, derived from  $z_{\parallel}$ ) and the membership signal ( $\cos(z_{\perp}, \mu_{\perp}^{(\hat{y})})$ ) have approximately decoupled failure modes. Confidence fails when OOD inputs produce high logits; membership fails when  $z_{\perp}$

accidentally aligns with the ID direction. These events are approximately independent ( $r=0.30-0.40$ , §4.5). Summing the two  $z$ -score-normalized signals provides OR semantics: *either* anomaly triggers detection. This is why *CORE* is robust where methods that see only one signal or both entangled, are brittle.

Our contributions are threefold:

- We identify orthogonal subspace decomposition of classifier features as a principled framework that explains *why* existing OOD methods are inconsistent—logit-based methods see only confidence ( $z_{\parallel}$ ), while feature-based methods measure membership entangled with confidence in the full  $z$ .
- We discover that the orthogonal residual  $z_{\perp}$  carries a class-specific directional signature that cleanly separates ID from OOD, providing a membership signal invisible to logit-based methods and entangled with noise in feature-based methods.
- *CORE* combines confidence and residual membership via  $z$ -score summation with  $\mathcal{O}(d)$  overhead, achieving the highest grand average AUROC (84.9%) across five model×dataset settings, ranking first in three of five, and never catastrophically failing where every baseline category does.

## 2 Related Work

We focus on post-hoc OOD detection methods that operate on pretrained classifiers without retraining. We organize prior work by how each method accesses the feature vector  $z$  and its derived quantities, and critique each category through the orthogonal decomposition  $z = z_{\parallel} + z_{\perp}$  introduced in §1.

### 2.1 Logit-Based Methods

The simplest family of post-hoc scorers operates solely on the classifier output  $\ell = Wz$ . MSP [10] uses the maximum softmax probability, while Energy [16] computes the log-sum-exp of logits. MaxLogit [1] directly uses the largest logit value, and ODIN [15] enhances MSP via temperature scaling and input perturbation. These methods are simple, require no training data, and are the most architecture-consistent category in our benchmarks. However, they share a fundamental blind spot: because  $\ell = Wz$  captures only the classifier-aligned component  $z_{\parallel}$ , any OOD sample that produces confident logits—*e.g.*, semantically near-OOD images—is invisible to these methods.

### 2.2 Feature-Based Methods

A second family computes scores from the penultimate feature  $z$  using statistics estimated from ID training data. Mahalanobis distance [14] fits class-conditional Gaussians and measures distance to the nearest class mean; its variant MDS++ [21] applies L2-normalization to improve conditioning. KNN [23] uses the  $k$ -th nearest neighbor distance in feature space, and CoP/CoRP [8] measure cosine similarity

between test features and class prototypes. These methods attempt to measure membership—whether a test sample belongs to the training distribution—by computing distances or densities in feature space. However, they operate on the full  $z$  without separating the confidence signal ( $z_{\parallel}$ ) from the membership signal ( $z_{\perp}$ ); the two remain *entangled*, and the full dimensionality of  $z$  introduces architecture-sensitive failure modes: Mahalanobis distance suffers from covariance collapse in high dimensions [21], and KNN is susceptible to *hubness*—a high-dimensional pathology where a few data points become nearest neighbors of disproportionately many others, causing OOD points to appear deceptively close to ID clusters. Our benchmarks show that feature-based methods exhibit the largest CNN-to-transformer performance gap among all categories, confirming their sensitivity to feature geometry.

### 2.3 Activation Shaping Methods

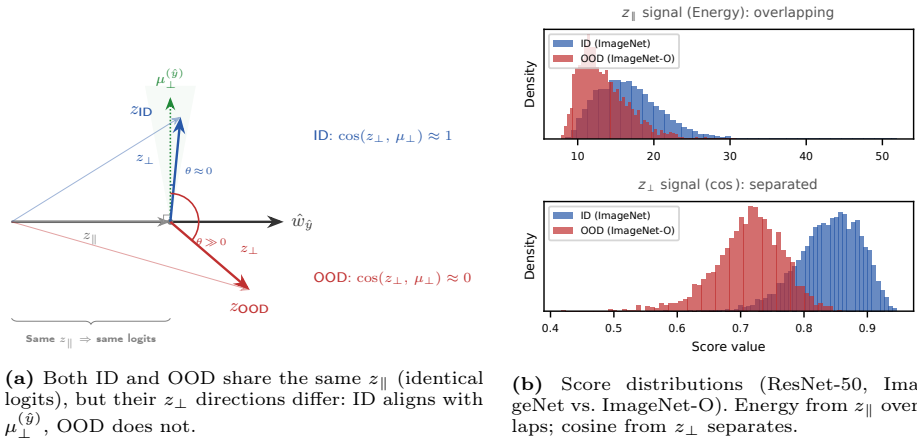
A third family modifies feature activations before recomputing logits. ReAct [22] clamps activations above a threshold, suppressing outlier magnitudes that OOD inputs tend to produce. ASH [6] zeroes out activations below a fixed percentile, and SCALE [28] prunes and exponentially rescales activations. These methods effectively denoise the feature vector to improve the logit-based signal. However, shaping rules calibrated for one architecture can be destructive for another: ASH assumes sparse activations (as produced by ReLU networks), but transformer features are uniformly distributed due to LayerNorm, causing ASH to drop to near-chance AUROC on ViT/ImageNet.

### 2.4 Hybrid Methods

Several methods compute a single score that inseparably mixes feature-based and logit-based quantities. ViM [26] projects features onto the classifier’s null space and combines the residual norm with an energy term; it comes closest to isolating membership by operating in the null space, but measures a *global* residual norm rather than a *class-conditional direction*, limiting its discriminative power. SHE [33] matches test features against memorized class-specific patterns via Hopfield energy. GradNorm [12] uses the gradient norm of the KL divergence between the softmax output and a uniform distribution. These methods produce a single indivisible score from features and logits jointly, so their failure modes cannot be isolated or corrected independently.

### 2.5 Score Combination Methods

A distinct family explicitly fuses separately defined component scores. NNGuide [19] multiplies the Energy score by a  $k$ -NN similarity weight, effectively using neighborhood density to gate classifier confidence. ComboOOD [20] sums Mahalanobis distance and  $k$ -NN scoring, fusing a parametric and a non-parametric distance measure. These are the closest in spirit to *CORE*—they recognize that a single



(a) Both ID and OOD share the same  $z_{\parallel}$  (identical logits), but their  $z_{\perp}$  directions differ: ID aligns with  $\mu_{\perp}^{(\hat{y})}$ , OOD does not.

(b) Score distributions (ResNet-50, ImageNet vs. ImageNet-O). Energy from  $z_{\parallel}$  overlaps; cosine from  $z_{\perp}$  separates.

**Fig. 3:** *CORE* decomposes features into classifier-aligned  $z_{\parallel}$  and orthogonal residual  $z_{\perp}$ . The residual carries a membership signal that is more discriminative than confidence alone and invisible to logit-based methods.

signal is insufficient and fuse complementary views. However, their fusion is *motivated but structurally fragile*: both methods extract their component signals from the same full feature  $z$ , so when the representation suffers from pathologies—covariance collapse in moderate dimensions or distance concentration (hubness) in high dimensions—both components degrade together (§4.5).

*Positioning.* *CORE* differs from all five categories by decomposing  $z$  into orthogonal subspaces  $z_{\parallel}$  and  $z_{\perp}$  and scoring each independently, yielding approximately independent failure modes by construction rather than by empirical coincidence.

### 3 Method

We present *CORE*, a scoring framework that decomposes penultimate features into two orthogonal subspaces and scores each independently. Figure 3 provides an overview.

#### 3.1 Problem Setup

Consider a pretrained classifier that maps an input image  $x$  to a predicted class  $\hat{y} \in \{1, \dots, C\}$ . The network consists of a feature extractor  $\phi: \mathbb{R}^m \rightarrow \mathbb{R}^d$  producing a penultimate feature  $z = \phi(x)$ , and a linear classifier with weights  $W \in \mathbb{R}^{C \times d}$  producing logits  $\ell = Wz \in \mathbb{R}^C$ . The predicted class is  $\hat{y} = \arg \max_c \ell_c$ .

Post-hoc OOD detection defines a scoring function  $S(x) \in \mathbb{R}$  such that higher values indicate in-distribution samples. A sample is classified as OOD when  $S(x) < \gamma$  for some threshold  $\gamma$ . The goal is to design  $S$  that is *consistently* discriminative across diverse architectures and datasets.

### 3.2 Orthogonal Feature Decomposition

The key observation behind *CORE* is that the classifier uses only a one-dimensional projection of  $z$  to compute the logit for any given class. For the predicted class  $\hat{y}$  with weight vector  $w_{\hat{y}} \in \mathbb{R}^d$  (the  $\hat{y}$ -th row of  $W$ ), the logit is  $\ell_{\hat{y}} = w_{\hat{y}}^\top z$ . This means the classifier’s decision depends only on the component of  $z$  aligned with  $w_{\hat{y}}$ , discarding the  $(d-1)$ -dimensional orthogonal complement.

We formalize this by decomposing  $z$  into two orthogonal components:

$$z = z_{\parallel} + z_{\perp}, \quad z_{\parallel} = \frac{z^\top w_{\hat{y}}}{\|w_{\hat{y}}\|^2} w_{\hat{y}}, \quad z_{\perp} = z - z_{\parallel}. \quad (2)$$

By construction,  $z_{\parallel}^\top z_{\perp} = 0$ . The parallel component  $z_{\parallel}$  encodes *confidence*: it determines the logit magnitude for the predicted class and, through cross-talk with other class weights, influences the full logit vector. The orthogonal residual  $z_{\perp}$  encodes everything the classifier ignores—we show next that it carries a *membership* signal.

### 3.3 Confidence Score: Energy

For the confidence component, we adopt the Energy score [16]:

$$S_{\text{conf}}(x) = \log \sum_{c=1}^C \exp(\ell_c) = \log \sum_{c=1}^C \exp(w_c^\top z). \quad (3)$$

Through the lens of our decomposition, Energy aggregates the projections of  $z$  onto all class weight directions. It is fundamentally a function of  $z_{\parallel}$  across the  $C$  class axes: it measures how strongly  $z$  aligns with the classifier’s learned directions overall. ID samples that activate class neurons strongly receive high Energy; OOD samples that fall between class directions receive low Energy. Energy is a well-established score [16]; our contribution is to reinterpret it as a confidence signal operating in the  $z_{\parallel}$  subspace and to complement it with an independent membership signal from  $z_{\perp}$ .

### 3.4 Residual Membership Score

We now present the core novel component of *CORE*. We discover that the orthogonal residual  $z_{\perp}$ —the part of  $z$  the classifier discards—is *structured* for ID data and *disrupted* for OOD data (Figure 3b).

*Observation.* Within each class  $c$ , ID samples’ residuals  $z_{\perp}$  tend to cluster around a consistent direction. Intuitively, samples of the same class share not only a similar projection onto the class weight (which determines their classification) but also similar “leftover” structure in the orthogonal complement—a class-specific signature that the classifier does not need for classification but that is characteristic of genuine class members. OOD samples misclassified as class  $c$  may match the projection (producing confident logits) but have arbitrary residual directions, since they were not drawn from the same data-generating process.

*Remark: connection to Neural Collapse.* The Neural Collapse phenomenon [18] predicts that well-trained classifiers drive within-class features toward their class mean along the classifier weight direction. Convergence is imperfect: a structured residual persists in  $z_{\perp}$ , reflecting within-class variation consistent across genuine class members. OOD inputs that mimic the class prototype along  $w_c$  may exhibit comparably concentrated residuals, but oriented in a different direction that does not match the class-specific signature  $\mu_{\perp}^{(c)}$ . We confirm this statistically across all five benchmark settings ( $p < 0.01$ , both CNNs and transformers; see supplementary). This explains why the directional signature is class-specific: each class occupies a distinct region of the orthogonal complement, shaped by the class-specific data distribution rather than the classifier weights.

*Offline estimation.* Given a small set of ID training samples for each class  $c$ , we compute the mean residual direction:

$$\mu_{\perp}^{(c)} = \text{normalize} \left( \frac{1}{|\mathcal{D}_c|} \sum_{x_i \in \mathcal{D}_c} z_{\perp,i} \right), \quad (4)$$

where  $\mathcal{D}_c$  is the set of training samples with label  $c$ , and  $z_{\perp,i}$  is the orthogonal residual of  $z_i = \phi(x_i)$  computed via Eq. (2).

*Online scoring.* For a test sample with predicted class  $\hat{y}$ , the membership score is:

$$S_{\text{mem}}(x) = \cos(z_{\perp}, \mu_{\perp}^{(\hat{y})}) = \frac{z_{\perp}^{\top} \mu_{\perp}^{(\hat{y})}}{\|z_{\perp}\|}. \quad (5)$$

ID samples yield high cosine similarity (their residuals align with the class-specific mean direction); OOD samples yield low similarity (their residuals point in arbitrary directions).

### 3.5 Score Combination

The confidence and membership scores operate on different scales: Energy typically ranges over  $[5, 30]$  while cosine similarity lies in  $[-1, 1]$ . We normalize each using  $z$ -score statistics computed from the ID training set:

$$S'_{\text{conf}} = \frac{S_{\text{conf}} - \mu_E}{\sigma_E}, \quad S'_{\text{mem}} = \frac{S_{\text{mem}} - \mu_R}{\sigma_R}, \quad (6)$$

where  $(\mu_E, \sigma_E)$  and  $(\mu_R, \sigma_R)$  are the mean and standard deviation of each score on the ID training data.

The final *CORE* score is their sum:

$$S_{\text{CORE}}(x) = S'_{\text{conf}} + S'_{\text{mem}}. \quad (7)$$

*Why summation.* The sum provides OR semantics: a sample is flagged as OOD if *either* its confidence is anomalously low *or* its residual direction is anomalous. This is the appropriate inductive bias because the two failure modes are complementary—confidence fails on OOD samples that produce high logits, while membership fails on OOD samples whose  $z_{\perp}$  accidentally aligns with the ID direction.

*Why principled.* Because  $z_{\parallel} \perp z_{\perp}$  by construction, the two scores are computed from orthogonal subspaces. This orthogonality provides a stronger guarantee than ad hoc score fusion: the failure modes of the two components are approximately independent—not merely empirically uncorrelated but grounded in the geometric separation of the subspaces ( $r=0.30\text{--}0.40$  on held-out data; §4.5); under Neural Collapse geometry, where class weights converge to an equiangular tight frame, the cross-talk between  $z_{\perp}$  and non-predicted class weights is further bounded. We verify this empirically in §4.5: the component scatter plots confirm that *CORE*’s signals occupy distinct regions of the score space, unlike other score combination methods whose components cluster along a shared diagonal (Figure 4).

Like MDS [14], KNN [23], and ViM [26], *CORE* requires a small set of ID training samples for offline estimation. Our main experiments use only  $\sim 13$  samples per class for ImageNet calibration ( $\sim 1\%$  of training data); §4.4 shows performance is stable from 1% to 100%. Computational cost is analyzed in §4.6.

## 4 Experiments

### 4.1 Setup

*Benchmarks.* We evaluate *CORE* across five benchmark settings spanning three CNN and two transformer architectures on two ID datasets: CIFAR-100 [13] with ResNet-18 [9] and WideResNet-40-2 [31]; and ImageNet [5] with ResNet-50 [9], ViT-B/16 [7], and Swin-B [17]. Each CIFAR-100 setting is evaluated against 8 OOD datasets and each ImageNet setting against 8, yielding 40 ID/OOD evaluation pairs in total.

*Baselines.* We compare against 16 post-hoc OOD scorers from five categories: *logit-based*—MSP [10], Energy [16], Max Logit [1]; *feature-based*—KNN [23], Mahalanobis [14], MDS++ [21], CoP [8], CoRP [8]; *activation shaping*—ReAct [22], ASH [6], SCALE [28]; *hybrid*—ViM [26], SHE [33], GradNorm [12]; *score combination*—NNGuide [19], ComboOOD [20].

*Metrics.* We report AUROC ( $\uparrow$ ) and FPR@95%TPR ( $\downarrow$ ), averaged across OOD datasets per setting. All scorers are post-hoc (no retraining); features are cached once per model and shared across all methods.

**Table 1:** Average AUROC (%) $\uparrow$ /FPR@95 (%) $\downarrow$  per setting. **Bold:** best. Underline: second-best. L=Logit, F=Feature, S=Shaping, H=Hybrid, C=Combination.

Method	Cat.	CIFAR-100		ImageNet			Avg.
		R18	WRN	R50	ViT	Swin	
MSP	L	78.2/79.2	74.4/83.7	78.8/72.5	79.9/68.2	85.0/51.6	79.2/71.0
Energy	L	80.3/76.5	77.2/81.9	82.0/67.7	79.3/ <u>60.7</u>	84.0/44.8	80.6/66.3
Max Logit	L	80.2/77.6	77.2/82.3	82.2/67.1	80.4/61.0	85.2/44.8	81.0/66.6
KNN	F	81.5/71.9	80.8/ <u>70.6</u>	73.0/69.5	44.8/97.7	83.6/68.6	72.7/75.6
Mahalanobis	F	66.3/89.7	77.5/76.3	63.6/83.6	77.2/84.1	87.9/53.8	74.5/77.5
MDS++	F	81.1/ <u>71.0</u>	<u>80.9</u> /73.2	82.5/58.2	<u>84.1</u> /63.6	89.3/45.0	<u>83.6</u> /62.2
CoP	F	71.4/79.7	57.4/90.5	76.0/66.0	68.1/85.8	88.2/45.8	72.2/73.5
CoRP	F	81.5/71.0	74.4/77.0	80.0/60.1	77.2/80.1	86.7/59.2	79.9/69.5
ReAct	S	80.4/74.5	75.9/80.0	86.2/ <b>49.9</b>	81.8/ <b>57.7</b>	86.7/ <u>41.4</u>	82.2/60.7
ASH	S	80.8/75.8	77.4/81.9	83.7/62.6	36.8/98.5	53.4/77.5	66.4/79.3
SCALE	S	81.4/74.1	78.1/78.7	<u>86.7</u> /52.0	71.0/72.8	85.0/44.8	80.4/64.5
ViM	H	80.3/76.3	78.5/76.6	82.4/67.8	77.4/79.1	<u>89.6</u> /47.2	81.6/69.4
SHE	H	78.4/77.5	60.9/87.0	82.5/56.2	78.6/66.0	79.9/51.7	76.1/67.7
GradNorm	H	70.3/77.3	50.2/93.6	81.7/54.9	51.8/90.3	39.3/87.1	58.7/80.6
NNGuide	C	81.5/74.6	79.0/77.7	85.9/ <u>50.7</u>	80.0/74.8	88.8/45.1	83.0/64.6
ComboOOD	C	<b>87.7</b> / <b>48.6</b>	<b>85.1</b> / <b>50.7</b>	76.7/66.4	71.2/71.3	81.7/56.7	80.5/ <b>58.7</b>
<i>CORE</i>	C	<u>82.1</u> /73.0	80.8/72.9	<b>86.7</b> /51.2	<b>84.3</b> /61.8	<b>90.7</b> / <b>37.2</b>	<b>84.9</b> / <u>59.2</u>

*Calibration data.* Like KNN [23] and NNGuide [19], several methods require ID training samples for offline calibration (*e.g.* fitting class prototypes,  $k$ -NN indices, or normalization statistics). For ImageNet, we provide a calibration set of  $\sim 1\%$  of training data; for CIFAR-100, the full training set. This lean budget tests robustness to limited calibration; §4.4 confirms that *CORE* is stable across budgets from 1% to 100%. All methods that require calibration share the same calibration set per setting, ensuring a fair comparison.

## 4.2 Main Results

Table 1 reports the average AUROC and FPR@95%TPR across OOD datasets for each of the five settings. Table 2 breaks down two representative settings by individual OOD dataset, grouped into near-OOD (semantically close to the ID data) and far-OOD.

*Overall.* *CORE* achieves the highest grand average AUROC (84.9%), ahead of MDS++ (83.6%) and NNGuide (83.0%), and ranks *first on all three ImageNet benchmarks*: R50 (86.7%), ViT (84.3%), Swin (90.7%)—no other scorer achieves this. The gain over Energy alone—which captures only the confidence signal that *CORE* also uses—is +4.7 (R50), +5.0 (ViT), and +6.7 (Swin) pp, demonstrating

**Table 2:** Per-OOD-dataset AUROC (%) for two representative settings. **Bold:** best. Underline: second-best. Near/far grouping follows OpenOOD [29].

(a) *ResNet-18 / CIFAR-100*

Method	Near-OOD		Far-OOD						Avg.
	C-10	TIN	SVHN	P365	LSUN	iSUN	Text	MNIST	
Energy	<u>79.2</u>	80.3	83.5	<u>77.3</u>	85.5	84.4	79.4	73.1	80.3
KNN	<u>77.1</u>	<b>81.2</b>	85.8	77.4	87.1	86.0	84.7	73.0	81.5
ViM	72.0	76.2	84.8	74.1	86.8	86.0	86.3	75.9	80.3
MDS++	71.6	74.8	<u>89.7</u>	75.1	86.2	86.2	<u>87.1</u>	<u>78.4</u>	81.1
NNGuide	<b>79.5</b>	<u>80.9</u>	84.8	<u>77.8</u>	<u>87.2</u>	<u>86.4</u>	82.2	73.2	81.5
ComboOOD	76.3	80.2	<b>97.9</b>	76.2	<b>99.0</b>	<b>98.5</b>	<b>92.3</b>	<b>81.5</b>	<b>87.7</b>
<i>CORE</i>	77.4	79.3	89.5	<b>78.1</b>	85.6	85.2	85.1	76.2	<u>82.1</u>

(b) *Swin-B / ImageNet*

Method	Near-OOD			Far-OOD					Avg.
	SSB	NINCO	ImgO	Places	SUN	iNat	Text	OImgO	
Energy	79.1	84.4	82.8	77.0	81.3	95.2	81.8	90.7	84.0
KNN	72.1	76.8	84.9	81.2	84.5	91.5	90.0	88.1	83.6
ViM	79.3	88.1	<u>93.4</u>	<u>84.3</u>	<u>86.6</u>	<b>99.1</b>	90.2	95.7	<u>89.6</u>
MDS++	<u>79.9</u>	<u>90.9</u>	93.3	80.8	82.9	<u>98.8</u>	91.2	<u>96.3</u>	89.3
NNGuide	77.3	88.1	93.0	82.4	84.7	98.1	91.0	96.0	88.8
ComboOOD	70.7	74.6	<b>96.5</b>	67.5	75.3	90.4	<b>92.4</b>	86.4	81.7
<i>CORE</i>	<b>83.1</b>	<b>90.9</b>	92.6	<b>85.0</b>	<b>87.9</b>	98.6	<u>91.4</u>	<b>96.4</b>	<b>90.7</b>

the large marginal value of the residual membership component on large-scale benchmarks. On CIFAR-100, ComboOOD leads (87.7% on R18, 85.1% on WRN) but catastrophically drops on ImageNet transformers:  $-16.5$  pp on ViT. Similarly, KNN drops  $-36.8$  pp and ASH drops  $-44.0$  pp from R18 to ViT. *CORE* **never catastrophically fails** (minimum: 80.8%), ranking first in three of five settings and remaining competitive in the other two.

*Per-dataset breakdown.* On Swin/ImageNet (Table 2b), *CORE* achieves the best AUROC on five of eight OOD datasets, with a notable near-OOD gain on SSB (+3.2 pp vs. runner-up MDS++) and a tie on NINCO (90.9%). ComboOOD leads on ImageNet-O (96.5%) and Textures (92.4%), and ViM on iNaturalist (99.1%); for *CORE* the gaps are small on these near-saturated benchmarks. On R18/CIFAR-100 (Table 2a), NNGuide leads on the hardest near-OOD split (C-10: 79.5%) while ComboOOD dominates far-OOD by a wide margin (e.g., LSUN: 99.0%, SVHN: 97.9%). *CORE* is consistently competitive across both groups, ranking first on Places365 (78.1%). The 5.6 pp gap to ComboOOD on R18 is driven entirely by far-OOD datasets (SVHN, LSUN, iSUN) where ComboOOD’s Mahalanobis+ $k$ -NN combination excels on low-dimensional CNN features—the same components that collapse on ImageNet transformers.

**Table 3:** Ablation studies (AUROC, %). (a) Component ablation: Confidence = Energy, Membership =  $\cos(z_{\perp}, \mu_{\perp}^{(i)})$ . (b) Combination function: all variants use  $z$ -score normalization.

	CIFAR-100		ImageNet			Avg.
	R18	WRN	R50	ViT	Swin	
<i>(a) Component ablation</i>						
Confidence only	80.3	77.2	82.0	79.3	84.0	80.6
Membership only	75.3	76.3	84.3	82.3	88.2	81.3
<b>CORE</b> ( $S'_{\text{conf}}+S'_{\text{mem}}$ )	<b>82.1</b>	<b>80.8</b>	<b>86.7</b>	<b>84.3</b>	<b>90.7</b>	<b>84.9</b>
<i>(b) Combination function</i>						
<b>Sum</b> (OR)	<b>82.1</b>	<b>80.8</b>	<b>86.7</b>	<b>84.3</b>	<b>90.7</b>	<b>84.9</b>
Softmin ( $\tau=5$ )	80.9	79.8	85.9	82.8	89.4	83.8
Max	79.9	79.0	84.2	83.3	87.3	82.7

**Table 4:** AUROC (%) vs. calibration budget for methods requiring initialization, averaged over 8 ImageNet OOD datasets.

Method	ResNet-50			ViT-B			Swin-B		
	1%	10%	100%	1%	10%	100%	1%	10%	100%
<b>CORE</b>	<b>86.7</b>	<b>87.4</b>	<b>87.5</b>	<b>84.3</b>	<b>85.1</b>	<b>85.1</b>	<b>90.7</b>	<b>90.9</b>	<b>91.0</b>
KNN	73.0	73.3	79.5	44.8	37.0	77.8	83.6	71.4	85.9
ViM	82.4	83.0	83.0	77.4	78.0	78.1	89.6	90.4	90.4
MDS++	82.5	83.9	83.9	84.1	84.8	84.8	89.3	90.1	90.2
NNGuide	85.9	85.3	84.6	80.0	80.6	79.5	88.8	89.7	89.5
ComboOOD	76.7	82.3	82.4	71.2	83.2	83.7	81.7	89.7	89.9

### 4.3 Ablation Study

Table 3(a) shows that the two components are complementary: membership alone surpasses Energy on all three ImageNet settings (+2.3 to +4.2 pp), confirming that  $z_{\perp}$  carries substantial discriminative signal in high-dimensional feature spaces. Conversely, confidence dominates on CIFAR-100 (+0.9 to +5.0 pp) where shallower features (512–640 dim) yield noisier residual estimates. Their combination exceeds the best single component on all 5 settings, with the largest gain on WRN (+3.6 pp) where both components are individually weak—precisely the setting where complementary fusion matters most. Table 3(b) compares combination functions: summation (OR semantics) consistently outperforms softmin and max (84.9% vs. 83.8% and 82.7%).

### 4.4 Sample Efficiency

Table 4 varies the calibration budget from  $\sim 1\%$  ( $\sim 13$  samples/class) to 100% for all methods requiring initialization. *CORE*'s AUROC changes by at most 0.8 pp

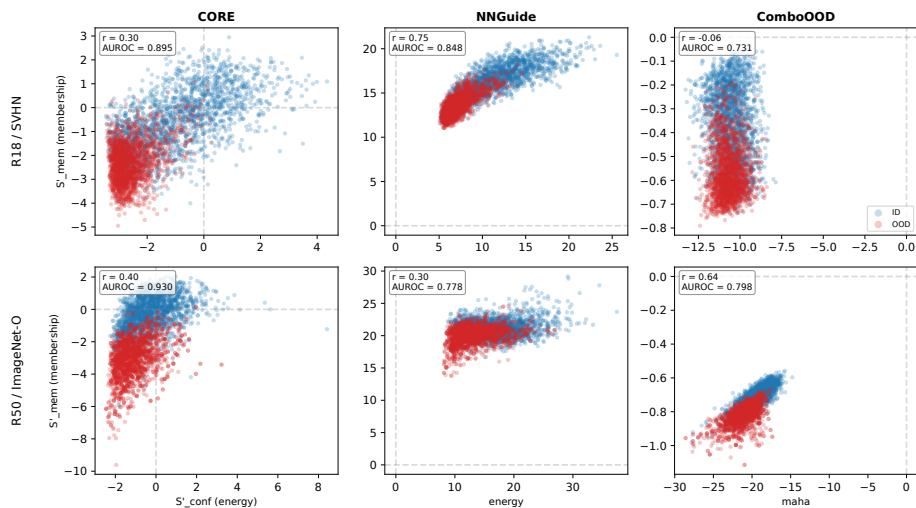


**Fig. 4:** Component scatter plots for three score combination methods on two representative settings (rows: R18/SVHN, R50/ImageNet-O). **Left:** *CORE*’s confidence ( $S'_{\text{conf}}$ ) and membership ( $S'_{\text{mem}}$ ) are weakly correlated ( $r=0.30, 0.40$ ); ID samples (blue) cluster at high values on both axes while OOD samples (red) scatter across complementary failure regions. **Center:** *NNGuide*’s energy and  $k$ -NN signals are entangled ( $r=0.75$  on R18) and overlap substantially. **Right:** *ComboOOD*’s Mahalanobis component collapses on CNN features (ID and OOD overlap entirely on the  $x$ -axis), and its  $k$ -NN component inherits hubness on ImageNet.

between 1% and 100% (Swin: 0.3 pp), because estimating a single mean direction  $\mu_{\perp}^{(c)}$  converges far faster than fitting  $d \times d$  covariance matrices (MDS++) or populating  $k$ -NN indices. KNN is catastrophically data-sensitive: on ViT it plummets from 77.8% (100%) to 44.8% (1%), and on Swin it exhibits a non-monotonic U-shape (83.6% at 1%, 71.4% at 10%, 85.9% at 100%), suggesting that intermediate budgets can actually *hurt* distance-based methods. *ComboOOD* is similarly unstable, dropping from 83.7% to 71.2% on ViT at 1%. Even at 1%, *CORE*’s grand average across the three ImageNet settings (87.2%) exceeds the 100%-data grand average of every competitor (MDS++: 86.3%, *ComboOOD*: 85.3%, *NNGuide*: 84.5%, ViM: 83.8%, KNN: 81.1%). This confirms that the residual direction is an inherently low-dimensional statistic: a single unit vector per class suffices.

#### 4.5 Analysis: Why *CORE* Is Robust

Figure 4 decomposes three score combination methods into their individual components. *CORE*’s confidence and membership signals are weakly correlated ( $r=0.30$  on R18/SVHN, 0.40 on R50/ImageNet-O): OOD samples that achieve high confidence but low membership—“confident misclassifications”—are caught by  $S'_{\text{mem}}$ , while the reverse case is caught by  $S'_{\text{conf}}$ . This low correlation is precisely what makes the combination effective: when one signal is fooled, the other

remains discriminative. In contrast, NNGuide’s two signals are structurally entangled ( $r=0.75$  on R18) because both derive from the full feature  $z$ , so the  $k$ -NN verification largely echoes what Energy already captures. ComboOOD’s components appear uncorrelated ( $r=-0.06$  on R18), but this is an artifact: the Mahalanobis component collapses to chance-level discrimination (AUROC 0.50) on CNN features, contributing noise rather than signal; on ViT,  $k$ -NN collapses instead (AUROC 0.36) due to hubness. *CORE*’s orthogonal decomposition avoids both failure modes: each component operates on a distinct subspace, yielding complementary signals whose combination is robust across all five settings.

#### 4.6 Computational Cost

*CORE* adds negligible overhead: given the penultimate feature  $z$  and predicted class  $\hat{y}$ , it requires two dot products ( $z^\top w_{\hat{y}}$  and  $z^\top \mu_\perp$ ), one vector subtraction, and two scalar  $z$ -score operations— $\mathcal{O}(d)$  per sample. Storage consists of  $\mu_\perp \in \mathbb{R}^{C \times d}$  and four normalization scalars ( $\mu_E, \sigma_E, \mu_R, \sigma_R$ )—for ImageNet ( $C=1000$ ,  $d=2048$ ), this is  $\sim 8$  MB. This is dramatically lighter than methods requiring  $\mathcal{O}(d^2)$  covariance matrices (Mahalanobis, MDS++) or  $\mathcal{O}(Nd)$  nearest-neighbor search (KNN, NNGuide). In contrast, the nearest competing score combination method requires forward hooks on *all* activation layers, a FAISS  $k$ -NN index over the full training set ( $\sim 10$  GB for ImageNet), and an inverse covariance matrix—orders of magnitude more compute and memory.

## 5 Conclusion

We showed that the inconsistency of post-hoc OOD scorers stems from entangling confidence and membership in the full feature space. *CORE* decomposes penultimate features into  $z_\parallel$  (confidence) and  $z_\perp$  (membership), combining two approximately independent signals via  $z$ -score summation. Across five model×dataset settings and 16 baselines, *CORE* achieves the highest grand average AUROC (84.9%) at  $\mathcal{O}(d)$  per-sample cost, with as few as  $\sim 1\%$  of training samples (§4.4). For practitioners, *CORE* offers a drop-in post-hoc scorer that requires no architecture-specific tuning, no covariance matrices, and no nearest-neighbor indices—only two dot products and one normalization per sample beyond a standard forward pass.

*Limitations.* *CORE*’s membership signal degrades on semantically extremely adjacent OOD data (e.g., CIFAR-10 vs. CIFAR-100,  $-2$  pp vs. NNGuide) where  $z_\perp$  shares the same directional structure as ID; this is inherent to any class-conditional membership method.

## References

1. Basart, S., Mantas, M., Mohammadreza, M., Jacob, S., Dawn, S.: Scaling out-of-distribution detection for real-world settings. In: International Conference on Machine Learning (2022)

2. Bitterwolf, J., Müller, M., Hein, M.: In or out? fixing ImageNet out-of-distribution detection evaluation. In: ICML (2023)
3. Cimpoi, M., Maji, S., Kokkinos, I., Mohamed, S., Vedaldi, A.: Describing textures in the wild. In: CVPR (2014)
4. Croce, F., Andriushchenko, M., Sehwag, V., Debenedetti, E., Flammarion, N., Chiang, M., Mittal, P., Hein, M.: Robustbench: a standardized adversarial robustness benchmark. In: Thirty-fifth Conference on Neural Information Processing Systems Datasets and Benchmarks Track (2021), <https://openreview.net/forum?id=SSKZPJct7B>
5. Deng, J., Dong, W., Socher, R., Li, L.J., Li, K., Fei-Fei, L.: Imagenet: A large-scale hierarchical image database. In: Proceedings of the IEEE/CVF Conference on Computer Vision and Pattern Recognition. pp. 248–255 (2009)
6. Djuricic, A., Bozanic, N., Ashok, A., Liu, R.: Extremely simple activation shaping for out-of-distribution detection. In: The Eleventh International Conference on Learning Representations (2023)
7. Dosovitskiy, A., Beyer, L., Kolesnikov, A., Weissenborn, D., Zhai, X., Unterthiner, T., Dehghani, M., Minderer, M., Heigold, G., Gelly, S., Uszkoreit, J., Houlsby, N.: An image is worth 16x16 words: Transformers for image recognition at scale. In: International Conference on Learning Representations (2021)
8. Fang, K., Tao, Q., Huang, K., Yang, X., Suykens, J.A.: Kernel pca for out-of-distribution detection. In: Advances in Neural Information Processing Systems. vol. 37 (2024)
9. He, K., Zhang, X., Ren, S., Sun, J.: Deep residual learning for image recognition. In: Proceedings of the IEEE Conference on Computer Vision and Pattern Recognition. pp. 770–778 (2016)
10. Hendrycks, D., Gimpel, K.: A baseline for detecting misclassified and out-of-distribution examples in neural networks. arXiv preprint arXiv:1610.02136 (2016)
11. Hendrycks, D., Zhao, K., Basart, S., Steinhardt, J., Song, D.: Natural adversarial examples. CVPR (2021)
12. Huang, R., Geng, A., Li, Y.: On the importance of gradients for detecting distributional shifts in the wild. *Advances in Neural Information Processing Systems* **34**, 677–689 (2021)
13. Krizhevsky, A., Hinton, G., et al.: Learning multiple layers of features from tiny images (2009)
14. Lee, K., Lee, K., Lee, H., Shin, J.: A simple unified framework for detecting out-of-distribution samples and adversarial attacks. In: Advances in Neural Information Processing Systems. vol. 31 (2018)
15. Liang, S., Li, Y., Srikant, R.: Enhancing the reliability of out-of-distribution image detection in neural networks. arXiv preprint arXiv:1706.02690 (2017)
16. Liu, W., Wang, X., Owens, J., Li, Y.: Energy-based out-of-distribution detection. *Advances in neural information processing systems* **33**, 21464–21475 (2020)
17. Liu, Z., Lin, Y., Cao, Y., Hu, H., Wei, Y., Zhang, Z., Lin, S., Guo, B.: Swin transformer: Hierarchical vision transformer using shifted windows. In: Proceedings of the IEEE/CVF International Conference on Computer Vision. pp. 10012–10022 (2021)
18. Pappayan, V., Han, X., Donoho, D.L.: Prevalence of neural collapse during the terminal phase of deep learning training. *Proceedings of the National Academy of Sciences* **117**(40), 24652–24663 (2020)
19. Park, J., Jung, Y.G., Teoh, A.B.J.: Nearest neighbor guidance for out-of-distribution detection. In: Proceedings of the IEEE/CVF International Conference on Computer Vision. pp. 1686–1695 (2023)

20. Rajasekaran, M., Sajol, M.S.I., Berglind, F., Mukhopadhyay, S., Das, K.: COM-BOOD: A semiparametric approach for detecting out-of-distribution data for image classification. In: Proceedings of the 2024 SIAM International Conference on Data Mining. pp. 643–651 (2024)
21. Ren, J., Fort, S., Liu, J., Roy, A.G., Padhy, S., Lakshminarayanan, B.: A simple fix to mahalanobis distance for improving near-ood detection. arXiv preprint arXiv:2106.09022 (2021)
22. Sun, Y., Guo, C., Li, Y.: React: Out-of-distribution detection with rectified activations. Advances in neural information processing systems **34**, 144–157 (2021)
23. Sun, Y., Ming, Y., Zhu, X., Li, Y.: Out-of-distribution detection with deep nearest neighbors. In: International Conference on Machine Learning. pp. 20827–20840. PMLR (2022)
24. Van Horn, G., Mac Aodha, O., Song, Y., Cui, Y., Sun, C., Shepard, A., Adam, H., Perona, P., Belongie, S.: The iNaturalist species classification and detection dataset. In: CVPR (2018)
25. Vaze, S., Han, K., Vedaldi, A., Zisserman, A.: Open-set recognition: A good closed-set classifier is all you need. In: ICLR (2022)
26. Wang, H., Li, Z., Feng, L., Zhang, W.: Vim: Out-of-distribution with virtual-logit matching. In: Proceedings of the IEEE/CVF Conference on Computer Vision and Pattern Recognition. pp. 4921–4930 (2022)
27. Xiao, J., Hays, J., Ehinger, K.A., Oliva, A., Torralba, A.: SUN database: Large-scale scene recognition from abbey to zoo. In: CVPR (2010)
28. Xu, K., Chen, R., Franchi, G., Yao, A.: Scaling for training time and post-hoc out-of-distribution detection enhancement. In: The Twelfth International Conference on Learning Representations (2024)
29. Yang, J., Wang, P., Zou, D., Zhou, Z., Ding, K., Peng, W.Z., Wang, H., Chen, G., Li, B., Sun, Y., Du, X., Zhou, K., Zhang, W., Hendrycks, D., Li, Y., Liu, Z.: OpenOOD: Benchmarking generalized out-of-distribution detection. In: NeurIPS (2022)
30. Yang, J., Zhou, K., Li, Y., Liu, Z.: Generalized out-of-distribution detection: A survey (2024), <https://arxiv.org/abs/2110.11334>
31. Zagoruyko, S., Komodakis, N.: Wide residual networks. arXiv preprint arXiv:1605.07146 (2016)
32. Zhang, J., Yang, J., Wang, P., Wang, H., Lin, Y., Zhang, H., Sun, Y., Du, X., Zhou, K., Zeng, W., et al.: OpenOOD v1.5: Enhanced benchmark for out-of-distribution detection. In: NeurIPS (2023)
33. Zhang, J., Fu, Q., Chen, X., Du, L., Li, Z., Wang, G., Liu, X., Han, S., Zhang, D.: Out-of-distribution detection based on in-distribution data patterns memorization with modern hopfield energy. In: The Eleventh International Conference on Learning Representations (2023)
34. Zhou, B., Lapedriza, A., Khosla, A., Oliva, A., Torralba, A.: Places: A 10 million image database for scene recognition. IEEE TPAMI **40**(6), 1452–1464 (2018)

## A Supplementary Material

### A.1 Implementation Details

*Architectures and layers.* Table 5 lists the penultimate and logit layer names, feature dimensionality, and input resolution for each architecture. All features are extracted as 1-D vectors after global average pooling (CNNs) or CLS token extraction (ViT) or spatial mean pooling (Swin).

**Table 5:** Architecture details.

Architecture	Penultimate	Logit	Dim	Size
ResNet-18	avgpool	fc	512	32
WRN-40-2	relu	fc	640	32
ResNet-50	avgpool	fc	2048	224
ViT-B/16	norm / vit.layernorm	head / classifier	768	224
Swin-B	swin.layernorm	classifier	1024	224

*Model sources.*

- **ResNet-18** (CIFAR-100): OpenOOD [32] pretrained checkpoint.
- **WRN-40-2** (CIFAR-100): RobustBench [4] Hendrycks2020AugMix\_WRN with built-in normalization.
- **ResNet-50** (ImageNet): torchvision pretrained (ImageNet-1K).
- **ViT-B/16** (ImageNet): timm vit\_base\_patch16\_224; (CIFAR): HuggingFace edumunozsala/vit\_base-224-in21k-ft-cifar100.
- **Swin-B** (ImageNet): HuggingFace microsoft/swin-base-patch4-window7-224.

*OOD datasets.* For CIFAR-100 experiments: CIFAR-10, Tiny ImageNet (resized to  $32 \times 32$ ), SVHN, Places365, LSUN (resized), iSUN, DTD Textures, MNIST (converted to RGB). For ImageNet experiments: SSB-Hard [25], NINCO [2], ImageNet-O [11], Places [34], SUN [27], iNaturalist [24], DTD Textures [3], OpenImage-O [26]. Near/far-OOD groupings follow OpenOOD [29]: for ImageNet, SSB-Hard, NINCO, and ImageNet-O are near-OOD; the remaining datasets are far-OOD.

*Calibration data.* For ImageNet settings, we use  $\sim 1\%$  of the training data ( $\sim 12,812$  samples) as calibration data for all methods requiring initialization. For CIFAR-100 settings, the full training set (50,000 samples) is used. All methods that require calibration share the same calibration set per setting.

**Table 6:** Neural Collapse verification: ID–OOD residual alignment gap  $\Delta$  across architectures. All gaps are positive and statistically significant.

Setting	Architecture	$\Delta$	95% CI	$p$ -value
CIFAR-100	ResNet-18	0.057	[0.052, 0.062]	$< 10^{-39}$
CIFAR-100	WRN	0.048	[0.044, 0.053]	$< 10^{-40}$
ImageNet	ResNet-50	0.086	[0.082, 0.090]	$< 10^{-152}$
ImageNet	ViT-B	0.267	[0.255, 0.279]	$< 10^{-157}$
ImageNet	Swin-B	0.325	[0.310, 0.339]	$< 10^{-152}$

## A.2 Neural Collapse Verification

We verify that the residual direction  $z_{\perp}$  carries a genuine membership signal by measuring the alignment gap  $\Delta = \mathbb{E}_{\text{ID}}[\cos(z_{\perp}, \mu_{\perp}^{(\hat{y})})] - \mathbb{E}_{\text{OOD}}[\cdot]$ . For each architecture, we compute class-specific mean residual directions  $\mu_{\perp}^{(c)}$  from correctly-classified training samples, then score both ID test and OOD samples by  $\cos(z_{\perp}, \mu_{\perp}^{(\hat{y})})$ . If Neural Collapse structures the orthogonal complement, ID residuals should align with  $\mu_{\perp}$  while OOD residuals should not, yielding  $\Delta > 0$ .

Table 6 confirms this across all five settings. The 95% confidence intervals are obtained via nonparametric bootstrap (10,000 resamples of the mean difference);  $p$ -values are from Welch’s  $t$ -test (unequal-variance, one-sided  $H_1: \mu_{\text{ID}} > \mu_{\text{OOD}}$ ). All CIs exclude zero and all  $p$ -values are astronomically small, confirming that the gap is not a statistical artifact. The gap is notably larger for transformers ( $\Delta=0.267$  for ViT-B, 0.325 for Swin-B) than for CNNs (0.048–0.086), suggesting that transformer features exhibit stronger class-specific structure in the orthogonal complement.

## A.3 Choice of Confidence Score

*CORE* uses Energy [16] as the confidence component  $S_{\text{conf}}$ . Table 7 replaces it with alternative logit-based scores to assess modularity. The membership component  $S_{\text{mem}} = \cos(z_{\perp}, \mu_{\perp}^{(\hat{y})})$  is fixed in all rows.

Energy is the best confidence component on all five settings, though Max Logit +  $S_{\text{mem}}$  performs comparably (84.8% vs. 84.9%). All three confidence scores improve substantially when combined with  $S_{\text{mem}}$ : MSP gains +0.4 to +6.2 pp, Max Logit +1.9 to +5.0 pp, confirming that the membership signal is complementary to *any* logit-based score. Energy is preferred as it marginally outperforms alternatives and is the most widely adopted confidence baseline [16].

## A.4 Component Correlation Analysis

Table 8 reports the Pearson correlation  $r$  between the  $z$ -score-normalized confidence  $S'_{\text{conf}}$  and membership  $S'_{\text{mem}}$  components of *CORE* across all five settings.

**Table 7:** Ablation: choice of confidence score (AUROC, %).  $S_{\text{mem}}$  is the residual membership component, shared across all combined variants.

Score	CIFAR-100		ImageNet			Avg.
	R18	WRN	R50	ViT	Swin	
<i>Confidence only (no <math>S_{\text{mem}}</math>)</i>						
MSP	78.2	74.4	78.8	79.9	85.0	79.2
Energy	80.3	77.2	82.0	79.3	84.0	80.6
Max Logit	80.2	77.2	82.2	80.4	85.2	81.0
<i><math>S_{\text{mem}}</math> only (no confidence)</i>						
$\cos(z_{\perp}, \mu_{\perp})$	75.3	76.3	84.3	82.3	88.2	81.3
<i>Confidence + <math>S_{\text{mem}}</math> (z-score sum)</i>						
MSP + $S_{\text{mem}}$	78.6	77.3	85.0	82.9	88.9	82.5
Max Logit + $S_{\text{mem}}$	82.1	80.7	86.7	84.2	90.2	84.8
<b>Energy + <math>S_{\text{mem}}</math> (CORE)</b>	<b>82.1</b>	<b>80.8</b>	<b>86.7</b>	<b>84.3</b>	<b>90.7</b>	<b>84.9</b>

**Table 8:** Pearson correlation between  $S'_{\text{conf}}$  and  $S'_{\text{mem}}$ .

Setting	Architecture	$r$ (ID)	$r$ (OOD avg.)
CIFAR-100	ResNet-18	0.08	0.07
CIFAR-100	WRN-40-2	0.49	0.30
ImageNet	ResNet-50	0.32	0.15
ImageNet	ViT-B	0.07	0.10
ImageNet	Swin-B	0.06	0.05

On four of five settings,  $|r| \leq 0.32$ , confirming that the two signals are approximately independent. The exception is WRN ( $r_{\text{ID}}=0.49$ ), whose wider architecture produces features with higher confidence–membership redundancy. This directly explains *CORE*’s weakest relative ranking on WRN (3rd, behind ComboOOD and MDS++): when  $S_{\text{conf}}$  and  $S_{\text{mem}}$  are correlated, their combination yields less complementary information, reducing the benefit of the dual-score design. Conversely, on transformers (ViT, Swin) where  $r < 0.10$ , *CORE* achieves its largest gains over single-signal baselines.

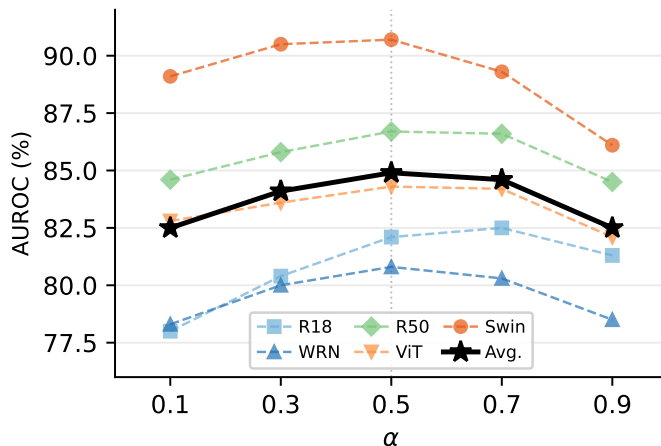
### A.5 Sensitivity to Hyperparameters

*CORE* has two design choices beyond the method itself: normalization mode, and the combination weight  $\alpha$  in  $S = \alpha S'_{\text{conf}} + (1-\alpha) S'_{\text{mem}}$ . We ablate each while fixing the others at their defaults (z-score,  $\alpha=0.5$ ).

*Normalization mode.* Table 9 compares z-score, min-max, and no normalization. z-score and min-max perform within 0.2 pp of each other (84.9 vs. 84.7), while omitting normalization drops performance by 2.8 pp. Normalization matters—but the specific choice does not.

**Table 9:** Normalization mode ablation (AUROC, %).

Normalization	CIFAR-100		ImageNet			Avg.
	R18	WRN	R50	ViT	Swin	
z-score	<b>82.1</b>	<b>80.8</b>	86.7	<b>84.3</b>	<b>90.7</b>	<b>84.9</b>
min-max	81.5	<b>80.8</b>	<b>86.8</b>	83.9	90.6	84.7
none	80.5	77.4	82.3	82.3	88.1	82.1

**Fig. 5:** Combination weight  $\alpha$  ablation.  $S = \alpha S'_{\text{conf}} + (1-\alpha) S'_{\text{mem}}$ . All settings peak near  $\alpha=0.5$  with a wide plateau.

*Combination weight  $\alpha$ .* Fig. 5 sweeps  $\alpha$  from 0.1 (membership-dominated) to 0.9 (confidence-dominated). Performance is remarkably flat across  $\alpha \in [0.3, 0.7]$  (84.1–84.9%), with  $\alpha=0.5$  at the peak. Only the extremes ( $\alpha=0.1$  or 0.9) degrade substantially ( $-2.4$  pp), confirming that equal weighting is a robust default requiring no tuning.

## A.6 Computational Cost

Table 10 compares the online scoring cost and offline storage of *CORE* against representative baselines on ResNet-50/ImageNet ( $d=2048, C=1000$ ). All timings are measured on a single NVIDIA A6000.

*CORE*'s online scoring requires only two dot products (projection + cosine), one subtraction, and two scalar operations per sample— $\mathcal{O}(d)$ , the lowest complexity among all methods that use features. Its storage (8 MB) consists of per-class residual directions  $\mu_{\perp}^{(c)} \in \mathbb{R}^{C \times d}$  and four normalization scalars, comparable to methods like SHE while substantially cheaper than KNN/NNGuide (105 MB train features) or Mahalanobis ( $d \times d$  precision matrix). Offline initialisation com-

**Table 10:** Computational cost comparison (ResNet-50 / ImageNet).

Method	Complexity	Latency (ms/samp)	Storage (MB)	Init
MSP / Energy	$\mathcal{O}(C)$	<0.001	0	—
ReAct / ASH / SCALE	$\mathcal{O}(Cd)$	<0.001	<0.1	Thr.
SHE	$\mathcal{O}(Cd)$	<0.01	8	$\mu_c$
ViM	$\mathcal{O}(d^2)$	$\sim 0.01$	8	Null sp.
Maha. / MDS++	$\mathcal{O}(d^2)$	$\sim 0.01$	32	$\Sigma^{-1}$
CoP	$\mathcal{O}(dq)$	<0.01	12	PCA
CoRP	$\mathcal{O}(dM)$	$\sim 0.05$	80	RFF+PCA
KNN / NNGuide	$\mathcal{O}(Nd)$	0.34	105	Train ft.
GradNorm	$\mathcal{O}(Cd)+\text{bkwd}$	$\sim 1$	0	—
<b>CORE</b>	$\mathcal{O}(d)$	<0.001	8	$\mu_{\perp}, \mu/\sigma$

putes  $\mu_{\perp}$  and  $z$ -score statistics from the calibration set in  $< 0.02$  s—orders of magnitude faster than KNN (index construction) or MDS (covariance inversion).

### A.7 Full Per-Dataset Results

The main paper (Table 2) reports per-OOD-dataset breakdowns for two representative settings (ResNet-18/CIFAR-100 and Swin-B/ImageNet). Here we provide the complete per-dataset AUROC (%) and FPR@95 (%) for all five settings. Near/far-OOD groupings follow OpenOOD [29]: for ImageNet, SSB-Hard, NINCO, and ImageNet-O are near-OOD; the remaining datasets are far-OOD. **Bold:** best; underline: second-best.

**Table 11:** Per-OOD-dataset AUROC (%) $\uparrow$  — ResNet-18 / CIFAR-100.

Method	Near-OOD		Far-OOD						Avg.
	C-10	TIN	SVHN	P365	LSUN	iSUN	Text	MNIST	
MSP	78.7	79.9	80.3	77.4	82.1	81.3	78.2	68.0	78.2
Energy	79.2	80.3	83.5	77.3	85.5	84.4	79.4	73.1	80.3
Max Logit	79.3	80.5	83.2	77.5	85.0	84.0	79.4	72.5	80.2
KNN	77.1	<b>81.2</b>	85.8	77.4	87.1	86.0	84.7	73.0	81.5
Mahalanobis	55.8	61.2	72.8	62.7	69.8	70.1	76.3	61.7	66.3
MDS++	71.6	74.8	89.7	75.1	86.2	86.2	<u>87.1</u>	78.4	81.1
CoP	57.7	61.2	82.9	61.1	74.4	75.3	80.4	78.0	71.4
CoRP	70.6	74.3	<u>91.0</u>	73.8	87.0	86.5	87.0	<b>81.6</b>	81.5
ReAct	75.4	79.2	82.6	<b>78.6</b>	<u>88.6</u>	<u>88.0</u>	85.7	65.0	80.4
ASH	79.3	80.3	84.4	77.5	85.8	84.8	80.1	73.8	80.8
SCALE	<u>79.4</u>	80.2	86.6	<u>78.2</u>	85.4	84.9	81.4	75.1	81.4
ViM	72.0	76.2	84.8	74.1	86.8	86.0	86.3	75.9	80.3
SHE	78.3	77.2	84.3	74.5	83.0	82.0	75.0	73.0	78.4
GradNorm	70.5	67.2	80.0	68.2	72.6	72.5	64.9	66.8	70.3
NNGuide	<b>79.5</b>	<u>80.9</u>	84.8	77.8	87.2	86.4	82.2	73.2	81.5
ComboOOD	76.3	80.2	<b>97.9</b>	76.2	<b>99.0</b>	<b>98.5</b>	<b>92.3</b>	<u>81.5</u>	<b>87.7</b>
<i>CORE</i>	77.4	79.3	89.5	78.1	85.6	85.2	85.1	76.2	<u>82.1</u>

**Table 12:** Per-OOD-dataset FPR@95 (%) $\downarrow$  — ResNet-18 / CIFAR-100.

Method	Near-OOD		Far-OOD						Avg.
	C-10	TIN	SVHN	P365	LSUN	iSUN	Text	MNIST	
MSP	79.9	75.7	79.4	80.0	73.0	75.5	79.7	90.5	79.2
Energy	79.6	<b>74.9</b>	76.6	80.4	66.0	68.6	77.4	88.4	76.5
Max Logit	<u>79.3</u>	75.4	77.6	80.0	68.9	71.5	78.5	89.4	77.6
KNN	80.9	<u>74.9</u>	62.4	<u>78.2</u>	61.6	66.0	63.6	88.1	71.9
Mahalanobis	95.8	94.4	91.5	93.2	87.4	84.6	73.4	97.6	89.7
MDS++	86.8	85.4	51.6	81.3	62.8	<u>60.3</u>	<u>53.8</u>	85.9	<u>71.0</u>
CoP	92.0	91.4	68.7	91.0	77.9	73.1	61.9	81.2	79.7
CoRP	88.4	86.8	<u>48.7</u>	84.8	65.1	63.5	55.3	<b>75.1</b>	71.0
ReAct	83.7	76.8	77.1	80.1	<u>59.8</u>	61.3	67.0	90.4	74.5
ASH	79.5	75.3	73.5	80.3	65.3	67.9	76.9	87.5	75.8
SCALE	<b>78.9</b>	75.4	65.7	<b>78.1</b>	66.8	68.8	73.8	85.5	74.1
ViM	87.8	85.1	74.2	84.0	64.8	64.5	59.5	90.5	76.3
SHE	80.0	80.2	68.0	82.5	72.2	72.9	80.4	84.1	77.5
GradNorm	80.6	79.7	70.2	81.8	71.5	71.9	79.0	84.0	77.3
NNGuide	80.8	75.3	72.8	80.1	61.3	64.4	73.1	88.8	74.6
ComboOOD	89.1	76.0	<b>11.4</b>	80.2	<b>5.2</b>	<b>7.6</b>	<b>38.6</b>	<u>80.5</u>	<b>48.6</b>
<i>CORE</i>	83.7	82.2	50.4	80.2	70.5	70.5	64.2	82.6	73.0

**Table 13:** Per-OOD-dataset AUROC (%) $\uparrow$  — WRN / CIFAR-100.

Method	Near-OOD		Far-OOD						Avg.
	C-10	TIN	SVHN	P365	LSUN	iSUN	Text	MNIST	
MSP	76.6	76.7	77.2	75.0	76.8	74.5	72.7	65.4	74.4
Energy	<u>78.7</u>	77.8	78.7	75.7	78.6	74.6	76.3	76.8	77.2
Max Logit	<b>78.9</b>	78.1	79.1	76.0	78.9	75.0	76.3	75.4	77.2
KNN	76.1	<b>79.7</b>	<u>90.7</u>	74.7	85.1	82.2	87.8	70.3	80.8
Mahalanobis	67.9	75.3	87.2	72.5	<u>86.1</u>	<u>85.0</u>	85.1	60.9	77.5
MDS++	75.8	77.1	89.3	74.5	80.1	78.9	<u>90.6</u>	80.7	<u>80.9</u>
CoP	49.6	48.5	63.0	44.5	49.4	52.4	77.5	74.2	57.4
CoRP	64.4	66.9	89.1	61.8	70.4	71.5	90.0	80.8	74.4
ReAct	70.0	75.9	80.2	<b>79.0</b>	82.5	80.4	83.3	55.7	75.9
ASH	78.6	77.4	79.6	75.1	77.1	73.2	78.8	79.6	77.4
SCALE	77.8	76.4	81.3	75.6	75.1	72.7	83.0	82.6	78.1
ViM	72.3	75.4	84.9	71.0	81.4	80.4	88.6	73.9	78.5
SHE	66.4	56.8	65.6	56.3	38.9	38.7	74.3	<b>89.8</b>	60.9
GradNorm	55.1	46.2	46.1	48.7	28.1	29.0	64.8	<u>83.8</u>	50.2
NNGuide	78.2	<u>78.2</u>	83.7	<u>76.8</u>	79.4	76.6	81.1	78.2	79.0
ComboOOD	70.2	74.8	<b>95.7</b>	72.1	<b>99.7</b>	<b>99.1</b>	<b>94.1</b>	75.2	<b>85.1</b>
<i>CORE</i>	76.9	78.2	88.5	75.4	78.6	76.7	90.1	81.8	80.8

**Table 14:** Per-OOD-dataset FPR@95 (%) $\downarrow$  — WRN / CIFAR-100.

Method	Near-OOD		Far-OOD						Avg.
	C-10	TIN	SVHN	P365	LSUN	iSUN	Text	MNIST	
MSP	80.7	80.7	82.9	83.0	81.2	84.2	85.2	91.5	83.7
Energy	<u>79.1</u>	78.4	84.8	81.2	82.2	86.6	82.8	79.7	81.9
Max Logit	79.5	78.7	83.9	81.7	81.4	86.1	83.4	83.5	82.3
KNN	82.7	<b>75.7</b>	<u>45.8</u>	81.2	69.7	71.8	51.0	86.5	<u>70.6</u>
Mahalanobis	91.3	84.2	61.1	85.9	<u>64.4</u>	<u>62.6</u>	61.6	99.0	76.3
MDS++	84.0	81.6	56.9	82.8	83.3	82.3	43.4	71.7	73.2
CoP	96.5	96.7	92.9	96.9	97.5	95.6	61.4	86.5	90.5
CoRP	91.5	89.1	54.0	91.5	89.6	86.8	<u>37.0</u>	76.8	77.0
ReAct	88.0	79.7	79.5	<b>77.3</b>	73.2	77.2	70.4	95.0	80.0
ASH	79.1	80.1	83.5	82.9	84.9	88.8	79.5	76.6	81.9
SCALE	<b>78.6</b>	79.1	77.8	81.4	84.0	87.0	68.7	73.2	78.7
ViM	86.9	82.6	67.2	86.0	75.0	72.9	50.6	91.3	76.6
SHE	88.6	93.8	90.8	95.1	98.9	98.6	72.5	<b>58.0</b>	87.0
GradNorm	94.0	97.0	98.4	97.0	99.4	99.3	84.9	78.8	93.6
NNGuide	79.2	<u>76.8</u>	73.7	<u>79.7</u>	79.2	83.6	72.6	76.8	77.7
ComboOOD	91.6	84.1	<b>22.6</b>	83.8	<b>1.7</b>	<b>3.5</b>	<b>28.0</b>	90.0	<b>50.7</b>
<i>CORE</i>	83.0	79.6	57.8	82.6	84.8	84.6	44.5	<u>66.1</u>	72.9

**Table 15:** Per-OOD-dataset AUROC (%) $\uparrow$  — ResNet-50 / ImageNet.

Method	Near-OOD			Far-OOD					Avg.
	SSB	NINCO	ImgO	Places	SUN	iNat	Text	OImgO	
MSP	70.7	79.9	69.8	79.0	80.1	88.2	78.9	83.8	78.8
Energy	70.3	79.5	75.0	82.1	84.9	91.3	84.9	88.3	82.0
Max Logit	70.7	80.3	74.9	82.2	84.8	91.6	84.6	88.3	82.2
KNN	49.3	60.2	89.1	64.7	72.2	84.1	92.8	71.2	73.0
Mahalanobis	46.2	60.2	86.0	51.1	49.8	57.6	91.1	66.5	63.6
MDS++	59.0	77.0	<u>95.3</u>	73.6	79.8	88.4	<b>98.6</b>	88.3	82.5
CoP	50.9	65.7	93.0	65.6	73.7	80.8	<u>97.8</u>	80.9	76.0
CoRP	53.9	71.4	<b>96.0</b>	71.9	78.6	86.6	97.8	83.4	80.0
ReAct	<u>71.6</u>	80.0	77.3	<b>91.6</b>	<b>94.1</b>	<b>96.5</b>	88.6	89.4	86.2
ASH	69.4	80.5	78.6	83.4	86.4	93.0	88.1	89.9	83.7
SCALE	<b>72.0</b>	<b>83.6</b>	82.4	<u>86.4</u>	<u>89.4</u>	<u>96.0</u>	91.5	<b>92.0</b>	<u>86.7</u>
ViM	63.1	78.5	91.4	76.2	78.4	86.5	96.9	88.3	82.4
SHE	68.3	75.5	79.5	81.9	86.3	92.8	90.3	85.1	82.5
GradNorm	67.2	73.2	78.6	82.2	87.5	94.1	87.9	83.1	81.7
NNGuide	70.9	82.2	81.0	85.9	88.9	95.5	91.9	91.0	85.9
ComboOOD	51.8	66.0	94.5	66.9	74.8	84.0	96.4	79.0	76.7
<i>CORE</i>	67.6	<u>82.5</u>	92.9	82.3	86.4	95.2	95.4	<u>91.1</u>	<b>86.7</b>

**Table 16:** Per-OOD-dataset FPR@95 (%) $\downarrow$  — ResNet-50 / ImageNet.

Method	Near-OOD			Far-OOD					Avg.
	SSB	NINCO	ImgO	Places	SUN	iNat	Text	OImgO	
MSP	85.9	76.6	80.3	75.6	72.9	52.4	70.1	66.3	72.5
Energy	85.6	76.8	77.4	70.1	64.2	49.5	57.9	59.9	67.7
Max Logit	85.1	75.2	77.2	69.4	65.0	46.5	59.2	59.2	67.1
KNN	94.3	89.4	52.6	84.7	76.0	56.8	29.6	72.3	69.5
Mahalanobis	97.1	95.5	61.6	97.3	97.1	95.2	38.0	86.9	83.6
MDS++	91.4	77.8	<u>27.1</u>	80.8	72.5	57.1	<b>6.9</b>	52.0	58.2
CoP	93.5	84.8	40.3	87.0	79.8	69.5	<u>10.6</u>	62.7	66.0
CoRP	91.9	82.3	<b>23.8</b>	80.8	71.6	59.4	10.9	60.3	60.1
ReAct	<b>79.4</b>	70.2	70.9	<b>35.7</b>	<b>26.0</b>	<b>18.3</b>	51.9	46.5	<b>49.9</b>
ASH	86.7	74.5	71.7	67.4	59.7	40.0	47.6	53.2	62.6
SCALE	83.2	<u>67.3</u>	62.6	57.0	47.9	<u>22.1</u>	34.1	<b>41.7</b>	52.0
ViM	92.4	81.9	44.5	85.0	85.3	76.4	14.7	62.4	67.8
SHE	85.2	72.6	64.5	60.6	49.1	31.1	34.3	52.0	56.2
GradNorm	84.5	73.8	66.5	56.6	<u>43.7</u>	24.5	38.9	50.6	54.9
NNGuide	<u>82.4</u>	<b>67.2</b>	61.6	<u>55.6</u>	45.2	22.1	30.0	<u>41.9</u>	<u>50.7</u>
ComboOOD	93.5	87.1	34.4	85.2	76.8	64.2	18.2	71.7	66.4
<i>CORE</i>	86.7	69.9	35.1	67.0	57.4	26.8	19.8	46.8	51.2

**Table 17:** Per-OOD-dataset AUROC (%) $\uparrow$  — ViT-B / ImageNet.

Method	Near-OOD			Far-OOD					Avg.
	SSB	NINCO	ImgO	Places	SUN	iNat	Text	OImgO	
MSP	69.1	79.4	78.8	79.7	81.2	88.7	77.7	84.4	79.9
Energy	<u>71.5</u>	77.8	78.9	77.1	81.3	87.4	79.4	81.2	79.3
Max Logit	71.0	79.4	79.6	79.0	82.0	89.3	79.2	83.4	80.4
KNN	43.4	42.6	36.9	42.3	44.0	50.2	54.6	44.1	44.8
Mahalanobis	62.3	76.1	81.8	70.9	72.0	90.2	77.1	87.0	77.2
MDS++	71.0	<b>84.5</b>	85.5	77.6	80.3	<b>95.3</b>	<u>86.7</u>	<b>91.5</b>	<u>84.1</u>
CoP	61.0	63.1	74.0	54.3	58.8	80.3	78.2	74.8	68.1
CoRP	63.4	75.9	80.6	70.8	72.6	86.2	84.3	83.6	77.2
ReAct	<b>72.7</b>	80.2	83.3	77.8	81.6	91.9	81.1	86.1	81.8
ASH	49.2	38.8	28.9	39.7	41.2	24.5	42.0	30.4	36.8
SCALE	68.6	69.9	63.6	70.5	76.6	76.4	73.1	69.3	71.0
ViM	62.5	74.5	84.5	68.0	70.4	91.8	79.5	87.9	77.4
SHE	69.4	76.5	77.0	<b>82.3</b>	<b>84.8</b>	79.5	84.5	75.0	78.6
GradNorm	60.3	51.8	45.4	52.4	56.6	47.0	55.8	45.0	51.8
NNGuide	65.6	77.7	82.6	78.8	81.0	85.6	85.0	83.8	80.0
ComboOOD	52.5	62.9	<b>87.4</b>	59.0	63.8	80.0	<b>88.3</b>	75.7	71.2
<i>CORE</i>	70.1	<u>83.5</u>	<u>87.1</u>	<u>81.8</u>	<u>84.4</u>	<u>92.4</u>	86.3	<u>88.9</u>	<b>84.3</b>

**Table 18:** Per-OOD-dataset FPR@95 (%) $\downarrow$  — ViT-B / ImageNet.

Method	Near-OOD			Far-OOD					Avg.
	SSB	NINCO	ImgO	Places	SUN	iNat	Text	OImgO	
MSP	84.6	72.0	69.3	71.2	67.6	49.9	70.2	60.6	68.2
Energy	75.4	66.7	59.2	<u>67.4</u>	<b>59.4</b>	47.4	57.3	53.1	<u>60.7</u>
Max Logit	78.9	67.0	59.4	<b>65.9</b>	<u>60.0</u>	43.0	61.4	52.8	61.0
KNN	98.3	98.3	98.5	99.0	99.0	98.0	92.3	98.0	97.7
Mahalanobis	92.4	86.9	84.7	90.5	91.9	71.1	85.6	69.5	84.1
MDS++	<u>75.3</u>	<u>66.6</u>	70.5	82.6	77.8	<b>28.3</b>	60.4	<u>47.5</u>	63.6
CoP	91.1	91.8	76.3	95.5	94.2	78.4	77.1	81.9	85.8
CoRP	89.5	84.5	74.0	90.0	89.5	73.4	67.1	72.6	80.1
ReAct	<b>74.8</b>	<b>65.0</b>	<u>53.1</u>	67.7	61.2	<u>36.0</u>	56.5	<b>47.1</b>	<b>57.7</b>
ASH	95.6	98.6	99.5	98.9	98.8	99.8	97.4	99.4	98.5
SCALE	76.5	75.4	80.4	77.2	68.7	67.8	67.7	68.6	72.8
ViM	90.8	85.0	77.7	88.6	88.8	58.1	80.7	62.8	79.1
SHE	80.8	73.4	66.6	67.9	62.6	59.4	<u>51.9</u>	65.0	66.0
GradNorm	85.9	91.1	92.7	92.8	90.9	93.5	85.9	89.3	90.3
NNGuide	88.3	82.0	75.2	77.8	75.6	75.1	57.4	66.7	74.8
ComboOOD	90.7	81.1	<b>50.3</b>	85.6	82.5	67.6	<b>43.0</b>	69.3	71.3
<i>CORE</i>	81.6	69.8	57.5	69.4	64.8	44.3	54.3	53.1	61.8

**Table 19:** Per-OOD-dataset AUROC (%) $\uparrow$  — Swin-B / ImageNet.

Method	Near-OOD			Far-OOD					Avg.
	SSB	NINCO	ImgO	Places	SUN	iNat	Text	OImgO	
MSP	76.4	85.8	80.6	82.7	84.3	94.8	83.8	91.3	85.0
Energy	79.1	84.4	82.8	77.0	81.3	95.2	81.8	90.7	84.0
Max Logit	78.8	85.9	82.5	80.1	83.4	95.7	83.5	91.8	85.2
KNN	72.1	76.8	84.9	81.2	84.5	91.5	90.0	88.1	83.6
Mahalanobis	75.0	86.9	90.9	84.1	85.4	98.6	88.2	94.5	87.9
MDS++	79.9	<b>90.9</b>	93.3	80.8	82.9	98.8	91.2	<u>96.3</u>	89.3
CoP	<u>82.4</u>	88.0	<u>95.4</u>	74.6	78.9	<u>99.0</u>	<u>92.3</u>	95.0	88.2
CoRP	77.7	86.2	91.8	78.2	80.5	95.7	89.8	93.5	86.7
ReAct	79.9	86.3	86.3	80.7	84.6	97.5	84.5	93.4	86.7
ASH	62.1	50.4	55.1	43.4	52.1	77.6	28.3	58.0	53.4
SCALE	79.0	85.2	83.9	79.1	82.7	95.9	82.2	92.1	85.0
ViM	79.3	88.1	93.4	<u>84.3</u>	<u>86.6</u>	<b>99.1</b>	90.2	95.7	<u>89.6</u>
SHE	74.4	82.6	87.9	59.2	63.1	92.5	90.1	89.7	79.9
GradNorm	54.5	45.9	33.7	30.9	34.5	33.7	38.0	43.2	39.3
NNGuide	77.3	88.1	93.0	82.4	84.7	98.1	91.0	96.0	88.8
ComboOOD	70.7	74.6	<b>96.5</b>	67.5	75.3	90.3	<b>92.4</b>	86.4	81.7
<i>CORE</i>	<b>83.1</b>	<u>90.9</u>	92.6	<b>85.0</b>	<b>87.9</b>	98.6	91.4	<b>96.4</b>	<b>90.7</b>

**Table 20:** Per-OOD-dataset FPR@95 (%) $\downarrow$  — Swin-B / ImageNet.

Method	Near-OOD			Far-OOD					Avg.
	SSB	NINCO	ImgO	Places	SUN	iNat	Text	OImgO	
MSP	70.2	51.9	59.0	61.5	57.9	22.9	54.1	35.1	51.6
Energy	<u>58.6</u>	44.8	46.4	59.6	51.3	15.5	53.8	28.3	44.8
Max Logit	62.6	45.1	49.6	57.2	51.5	15.4	49.9	27.4	44.8
KNN	78.7	82.5	72.1	81.1	69.6	58.3	44.0	62.3	68.6
Mahalanobis	81.4	68.1	52.8	69.0	68.5	6.2	51.1	33.0	53.8
MDS++	60.8	44.2	36.4	80.3	77.5	5.8	33.8	21.5	45.0
CoP	<b>58.4</b>	53.0	<u>26.8</u>	84.6	78.3	<u>5.2</u>	<b>32.2</b>	27.8	45.8
CoRP	73.4	67.7	51.1	85.5	82.8	30.2	41.6	41.5	59.2
ReAct	59.0	<u>43.8</u>	41.5	<u>55.6</u>	<b>47.6</b>	10.0	50.0	23.5	<u>41.4</u>
ASH	82.3	82.7	80.3	88.2	81.6	44.7	97.0	63.6	77.5
SCALE	60.4	45.5	46.5	58.6	51.5	14.6	54.2	26.9	44.8
ViM	75.2	61.8	40.5	65.9	63.2	<b>3.1</b>	42.9	25.0	47.2
SHE	68.4	55.0	47.0	75.1	72.4	24.6	36.2	35.2	51.7
GradNorm	80.4	81.9	91.4	92.6	89.1	88.8	92.6	79.5	87.1
NNGuide	70.7	53.4	36.4	70.2	68.3	8.5	33.6	<u>20.2</u>	45.1
ComboOOD	79.5	72.5	<b>18.6</b>	81.2	72.7	43.7	<u>32.6</u>	52.6	56.7
<i>CORE</i>	58.7	<b>40.8</b>	35.8	<b>54.9</b>	<u>47.9</u>	6.4	35.7	<b>17.7</b>	<b>37.2</b>